Available online at www.sciencedirect.com

SciVerse ScienceDirect

Ceramics International 39 (2013) 6599–6606

CERAMICS INTERNATIONAL

www.elsevier.com/locate/ceramint

Facile solvothermal synthesis and polarity based tunable morphologies of ZnO nanocrystals

Jin Young Park[a], Hong Chae Jung[a], G. Seeta Rama Raju[b], Byung Kee Moon[a,*], Jung Hyun Jeong[a], Hae Young Choi[c], Jung Hwan Kim[c]

[a]Department of Physics, Pukyong National University, Daeyon 3-dong, Nam-gu, Busan 608-737, Republic of Korea

[b]Department of Electronics and Radio Engineering, Kyung Hee University, 1 Seocheon-dong, Giheung-gu, Yongin-si, Gyeonggi-do 446-701, Republic of Korea

[c]Department of Physics, Dong Eui University, Gaya-dong, Busan-Jin-gu, Busan 617-714, Republic of Korea

Received 11 January 2013; received in revised form 28 January 2013; accepted 28 January 2013
Available online 4 February 2013

Abstract

ZnO nanoparticles (NPs) with rod, bullet and broom-like morphologies have been synthesized by the solvothermal method. Structural analysis revealed ZnO NPs to be of the single crystal wrutzite hexagonal structure. Their size and morphology were controlled by varying the polarity of solvents. The aspect ratio of ZnO NPs at the lower polarity was below 2, and their shape was like a bullet. When increasing the polarity of solvent, the aspect ratio also increases and the shape changes to a rod-like morphology. This process is very simple and scalable. In addition, it can be used for fundamental studies of the tunable morphology formation.

Keywords: D. ZnO; Crystal growth; Solvothermal; Polarity

1. Introduction

Nowadays, the development of nanocrystalline materials with controllable size and shape with different dimensions (zero, one, two and three) has not only attracted a great deal of attention owing to their superior physical and chemical properties, but also offers an opportunity to study and imitate their biological function at the nanoscale level [1–9]. The physical and chemical properties of nanomaterials depend upon the size and shape, but the production of nanomaterials with specific size and shape is still a significant challenge. Hofmann et al. synthesized the iron oxide and iron manganese oxide with shapes of nanotetracube and star-like by the aid of surfactant [10]. Joo et al. also synthesized the cone, hexagonal cone and rod shape morphologies of ZnO nanocrystals using a surfactant by means of the sol–gel process [11]. However, it is difficult to completely remove the surfactant without collapse of the morphology. Currently, in order to overcome this shortcoming, a large number of soft chemistry routs without a surfactant have successfully been developed for the synthesis of simple binary metal oxide nanostructures such as TiO_2, ZrO_2, SiO_2 and ZnO [12–16].

Among the various binary metal oxide materials, ZnO is one of the most important oxide semiconductor materials with a wide band-gap energy of 3.37 eV and large exciton binding energy of 60 meV, which is much larger than other semiconductor materials such as GaN (25 meV) and ZnSe (22 meV). It has gained much considerable attention due to its wide range of potential applications in sensors, field emission displays, dye-sensitized solar cells, photoinduced switching devices, phosphors, light emitting diodes (LED), photocatalytic activity and so on [16–20]. By focusing on these advantages, different morphologies of ZnO have been prepared by various physical, chemical and electrochemical methods such as thermal evaporation, metal–organic vapor phase epitaxy, pulsed laser deposition, chemical synthesis and electrochemical deposition [21–25]. Wu et al. reported the low-temperature growth of ZnO nanorod by the chemical

*Corresponding author. Tel.: +82 51 629 5569; fax: +82 51 629 5549.
E-mail address: bkmoon@pknu.ac.kr (B.K. Moon).

0272-8842/$ - see front matter © 2013 Elsevier Ltd and Techna Group S.r.l. All rights reserved.
http://dx.doi.org/10.1016/j.ceramint.2013.01.095

vapor deposition method [26]. Bai et al. prepared the ZnO nanostructures with flower and bruch pen-like morphologies by the hydrothermal method [27], and using the similar method, Ko et al. synthesized the ZnO nanowires [28].

Among the various synthetic routes, the hydrothermal method is a powerful option to synthesize the tunable morphology and obtain the large-scale production of nanomaterials due to its simple procedure, fast growth, and lower cost. The solvothermal method is similar to the hydrothermal method, in which other solvents are used instead of water. The nature of solvent plays an imperative role on the crystal formation and its morphology. Sathis et al. reported the size tunable fullerene (C_{60}) by controlling the solvents such as MeOH, EtOH, isopropyl alcohol and toluene [29]. They control the diameter of C_{60} nanosheet with different chain lengths of the solvents. When the chain length of the solvent is decreased, the diameter of nanosheets is increased. However, so far, no other reports have been found on the effect of polarity of solvents in growing ZnO nanostructures. In this paper, we report on the shape control of the ZnO nanoparticles as a function of reaction parameters such as reaction time and polarity of solvents.

2. Experimental section

2.1. Solvothermal synthesis

The ZnO NPs were fabricated by the solvothermal reaction method at a reaction temperature of 250 °C. All the chemical reagents were of analytical grade. In a typical procedure, 0.1 M zinc acetylacetonate ($Zn(AcAc)_2$, $Zn(C_5H_7O_2)_{2-x}\cdot H_2O$, 99.99 %, Aldrich) was added to 40 mL of various solvents. The solution was transferred

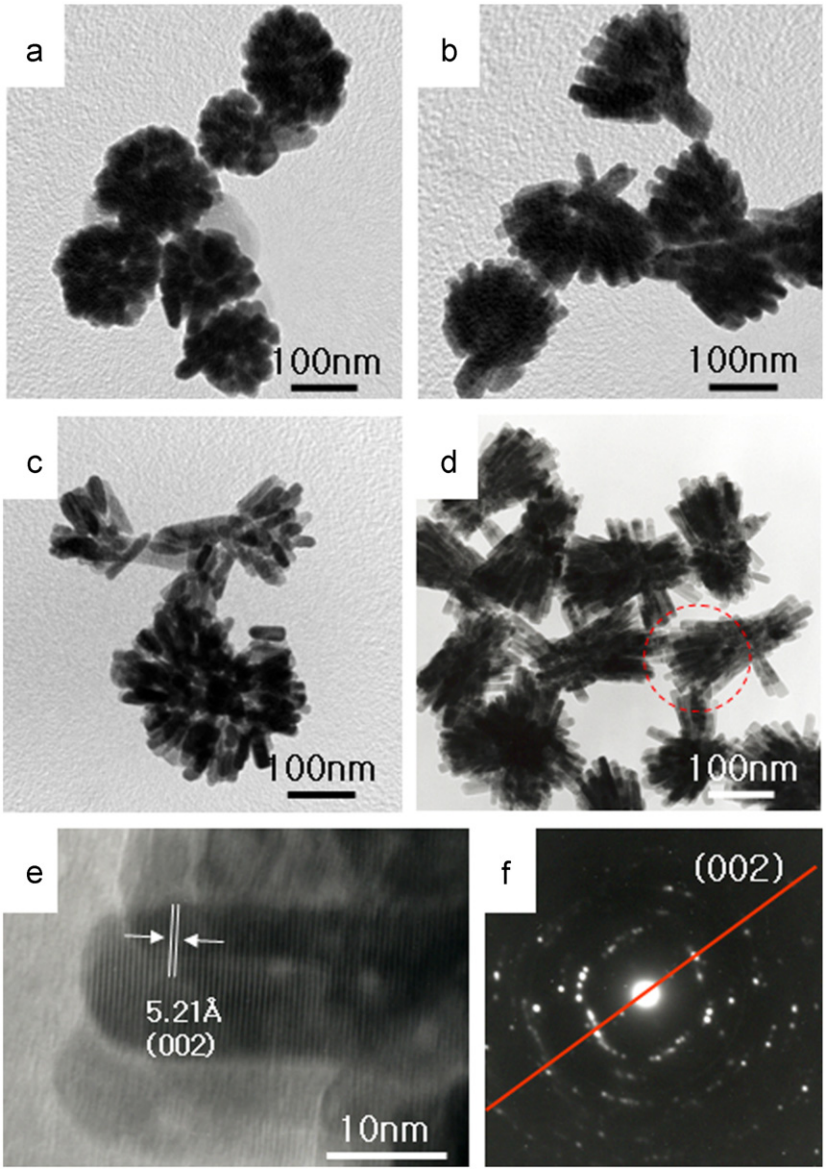

Fig. 1. SEM and TEM images of the ZnO NPs synthesized by the solvothermal reaction in 2-PrOH at 250 °C: (a) 5 h, (b) 10 h, (c) 15 h, (d) 20 h, (e) high resolution TEM image from a circle in (d), and (f) SAED pattern from the same circled area in (d).

into a stainless steel autoclave (total inner volume of 80 cm^3) with a Teflon liner (80 cm^3 volume with 50% filling). The solution was heated to 120 °C at a rate of 2 °C/min and held at this temperature for 1 h with magnetic stirring. The reaction temperature was then raised from 120 to 250 °C at a rate of 2 °C/min and held at this temperature without magnetic stirring. The precipitate of ZnO NPs was formed at the bottom of the Teflon liner. After gradually cooling down to room temperature, the precipitate was washed separately with ethanol and water. The obtained precipitate was dried at 60 °C for a day in the ambient atmosphere.

2.2. Characterization

The structure of the prepared ZnO NPs was analyzed with a powder X-ray diffraction (XRD) using X'PERT PRO diffractometer with CuKα = −1.5406 Å and beam voltage of 40 kV and 30 mA beam current. The morphology and size were examined by using a field emission scanning electron microscopy (FE-SEM), model JEOL JSM-6700 FESEM. Osmium coating was sprayed on the sample surfaces by using Hitachi fine coat ion sputter E-1010 unit to avoid possible charging of the specimens before FESEM observation was made on each time. Transmission electron microscopy (TEM) studies were carried out using a JEOL JEM-2010 operating at an accelerating voltage of 200 KV. The sample was prepared by dispersing the ZnO NPs in ethanol and then the dispersion solution was dropped on a carbon coated copper grid and dried in an ambient atmosphere.

3. Results and discussion

3.1. Effect of reaction time

One of the important factors in the growth process is the reaction time. In order to study the formation process of the ZnO NPs, the growth process has been followed by extracting the product as a function of reaction time (5, 10, 15 and 20 h) by keeping the reaction temperature constant at 250 °C and the resultant products have been studied by TEM measurements. Fig. 1 shows the TEM images of the ZnO NPs synthesized by the solvothermal reaction at various reaction times from 5 to 20 h. After 5 h of solvothermal reaction, amorphous nanoparticles with 10 nanometer sized were collected (Fig. 1a). When the reaction time extended to 10 h, the broccoli-like ZnO NPs consisting of nanorods with an average diameter of 30 nm and an average length of 100 nm were obtained, but their morphologies were not clear in Fig. 1b. The reaction time further extended to 15 h, as can be seen in Fig. 1c, ZnO nanorods with 100 nm length and 30 nm diameter and the clear morphology including edges were observed. Finally,

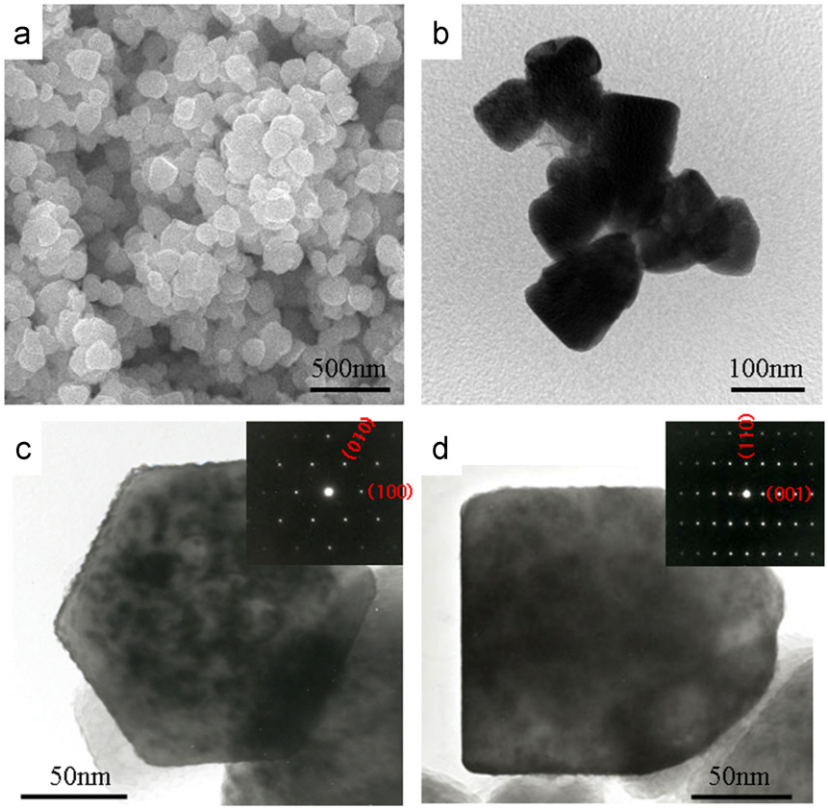

Fig. 2. (a) SEM image of the ZnO NPs synthesized by a solvothermal reaction in toluene at 250 °C for 20 h, (b) TEM image, (c) high magnificent TEM image of bullet-like ZnO attached with its bottom wall plane (inset is the SAED pattern of bottom wall plane), and (d) high magnificent TEM image of bullet-like ZnO attached with its side wall plane (inset is the SAED pattern of side wall plane).

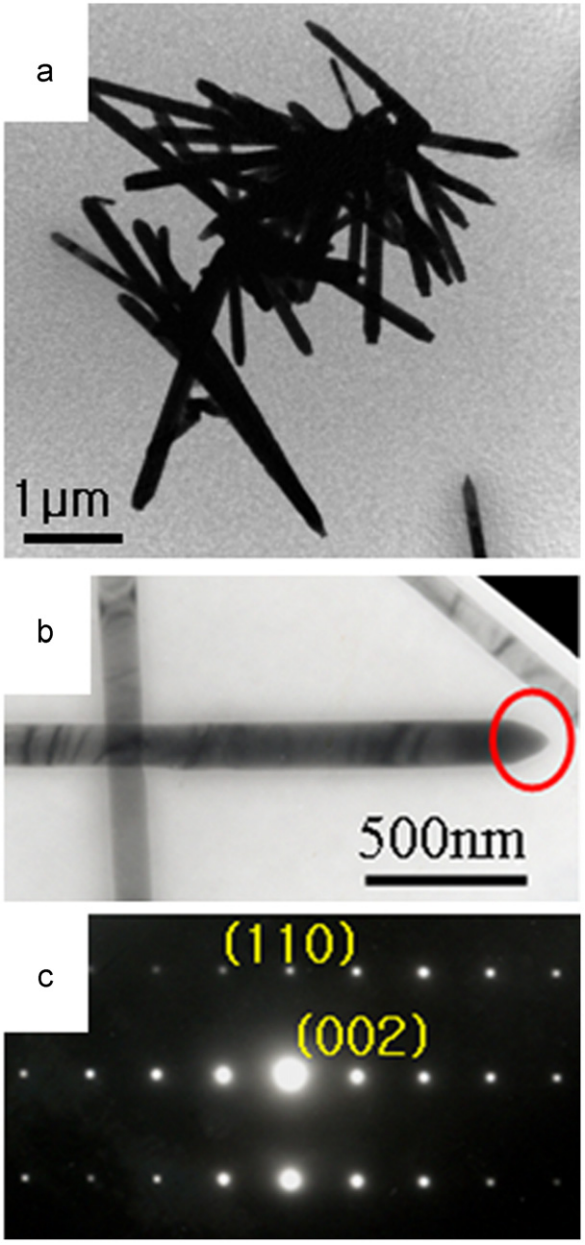

Fig. 3. TEM images of the ZnO NPs synthesized in water at 250 °C for 20 h: (a) TEM image, (b) magnification of TEM image, and (c) SAED pattern from the same circled area in (b).

when the reaction time was increased to 20 h, well crystallized broom-like morphologies of ZnO nanorods were developed (Fig. 1d), and the average diameter and length of each nanorod was about 30 nm and 200 nm, respectively. Fig. 1e shows the high-resolution TEM (HR-TEM) image, which was taken from the highlighted circular area in Fig. 1d. The lattice spacing of around 5.21 Å, which corresponds to the *d*-spacing of (002) plane was verified by wurtzite hexagonal structure and grown along the *c*-axis direction. No dislocations were observed in this area, the edges of ZnO NPs are clear and no amorphous layer was observed on the surface. Fig. 1f shows the selected area electron diffraction (SAED) pattern. The SAED pattern indicates that the particle has a single-crystal structure and confirms the growth direction, which is along the *c*-axis.

3.2. Effect of polarity of solvent

The key factor in the growth procedure is the solvent, which has been considered to investigate the morphology and shape of ZnO NPs. In order to study the various morphologies and shapes of the ZnO NPs, the solvents having different kinds of polarities were used at the same reaction temperature of 250 °C and time 20 h. Fig. 2 shows the TEM images of the ZnO NPs synthesized in the toluene by the solvothermal reaction at 250 °C for 20 h. Fig. 2a and b are a low magnification SEM and TEM images showing the uniformity of the nanostructure. Fig. 2c and d shows a high magnification TEM image of a bullet-like ZnO single particle attached with its bottom wall plane and its side wall plane, respectively. The inset of Fig. 2c and d shows the SAED pattern, which clearly indicates that the whole particle has a single crystal structure. From the SEM and TEM images, the bullet-like morphology with the average diameter and lengths between 80–100 nm and 100–130 nm, respectively were observed.

Fig. 3 shows the TEM images of the ZnO NPs synthesized in distilled water, and other conditions are constant. Fig. 3a and b shows the TEM images, which revealed that the diameter and length of the particles are about several micrometers. The edges of the ZnO rods are clear, and no amorphous layers were observed. Fig. 3c shows the SAED

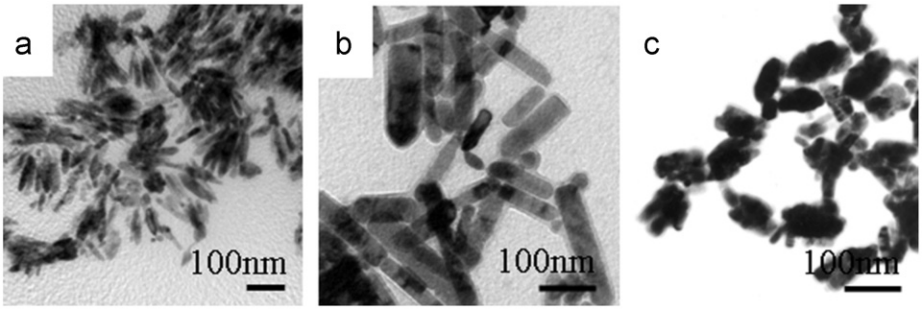

Fig. 4. TEM images of the ZnO NPs synthesized by a solvothermal reaction in polar solvents at 250 °C for 20 h: (a) ethanol, (b) pyridine, and (c) 2-methoxyethanol.

pattern, which confirmed that the ZnO NPs grown in water also has a single crystalline nature. The SAED pattern approved that the ZnO rods growing along the *c*-axis. The ZnO NPs synthesized with higher polarity solvent (toluene: 2.4 < 2-PrOH: 3.9 < water: 10.2), the length growing is faster than that of diameter when compared with toluene. The aspect ratio also increased with increasing the polarity. Other ZnO NPs synthesized in polar solvents with polarity between 5 and 5.5, and a non-polar solvent with lower polarity of 3 is presented in Figs. 4 and 5, respectively. All ZnO NPs grown in a non-polar solvent show the lower aspect ratio (< 2) and show higher aspect ratio (2–4) when grown in polar solvents.

Furthermore, in order to investigate the effect of solvents, we synthesized ZnO NPs by using toluene/2-PrOH and 2-PrOH/water interfaces and other conditions are kept constant. Fig. 6 shows the XRD patterns of the ZnO NPs prepared with mixed solvents of toluene and 2-PrOH. All ZnO NPs are wrutzite structure and diffraction peaks are indexed to a hexagonal structure (JCPDS card No. 36-1451). It is clear that the (002) peak intensity and the full-width at half-maximum (FWHM) of the (100) peaks are increased by increasing the 2-PrOH content, suggesting that the ZnO NPs were grown in the direction of *c*-axis more than the direction of (100). The crystallite size was estimated by using Scherrer's equation and the full-width at half-maximum (FWHM) was selected for the major diffraction peaks [30]. The calculated average crystallite sizes were about 38.3, 24.4, 18.5, 17.0 and 13.7 nm for the samples prepared using toluene/2-PrOH

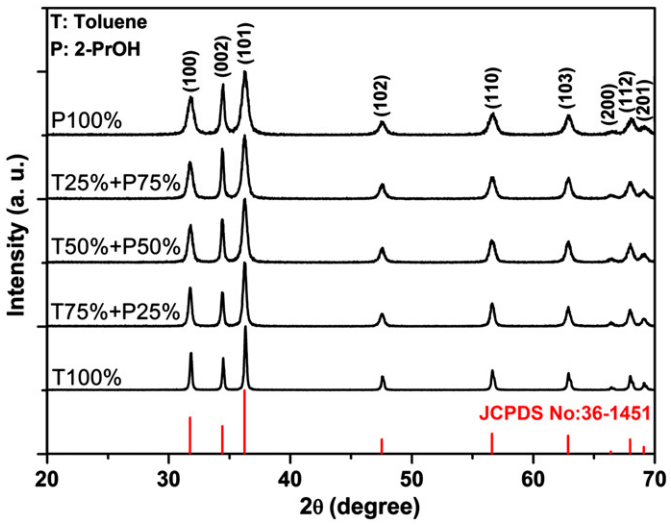

Fig. 6. XRD of ZnO NPs at different toluene/2-PrOH interface.

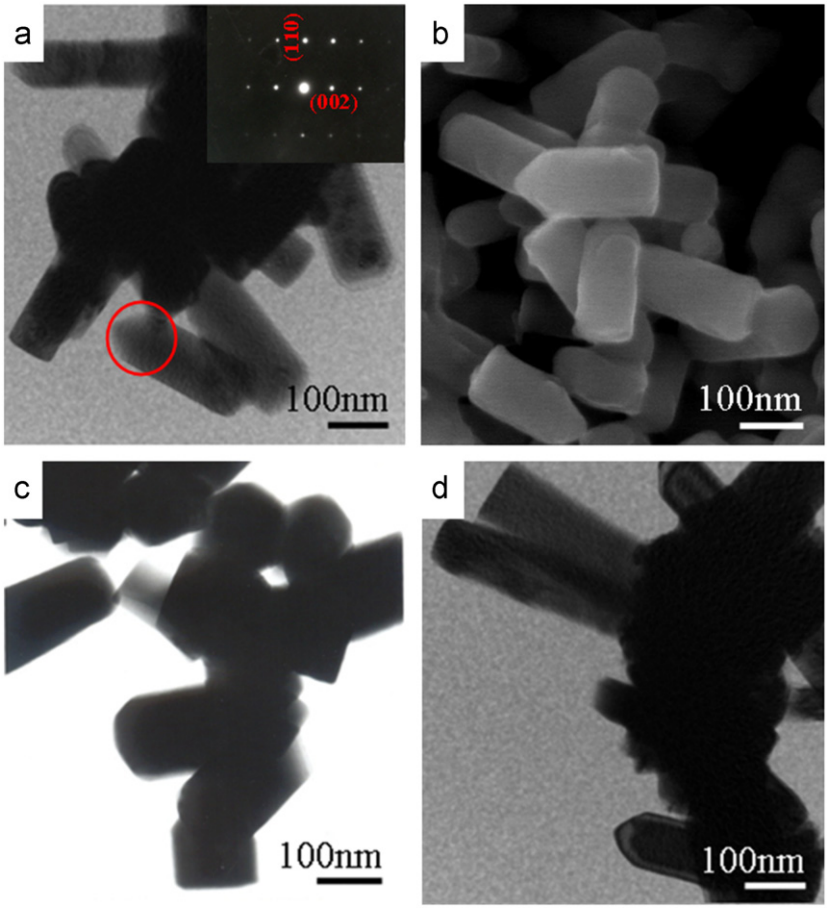

Fig. 5. ZnO NPs synthesized by a solvothermal reaction in non-polar solvents at 250 °C for 20 h: (a) TEM image, (b) SEM image of ZnO grown in cyclohexane, (c) ZnO grown in toluene, and (d) ZnO grown in benzene. The inset of (a) shows the corresponding SEAD pattern taken on the circled area in a.

interface (100:0), (75:25), (50:50), (25:75) and (0:100), respectively.

Fig. 7 shows the TEM images of the different percentages of the toluene and 2-PrOH interface (100:0), (75:25), (50:50), (25:75) and (0:100). Fig. 7a shows the bullet-like ZnO NPs synthesized in toluene. As expected, when the 2-PrOH content increases to 50%, the diameter of ZnO NPs decreased and the aspect ratio increases (Fig. 7c–e). When the 2-PrOH content was extended to 75%, the agglomeration begins. Finally, when the 2-PrOH content was extended to 100%, the broom-like ZnO NPs consisting of nanorods were observed. In toluene/2-PrOH interface, it was found that the diameter decreased and the aspect ratio increases with an addition of 2-PrOH content (the polarity of 2-PrOH is higher than that of toluene), which has been represented in Fig. 7f. The above observation indicates that the aspect ratio increases with increasing the 2-PrOH content. This exhibits the effect of 2-PrOH and speculates that the 2-PrOH is a much more polar molecule than toluene. In order to better understand, the ZnO NPs prepared in 2-PrOH/water interfaces presented in Fig. 8. Fig. 8 shows the TEM images of the different percentages of 2-PrOH and water interface (100:0), (95:5), (87.5:12.5), (75:25), (50:50) and (0:100). With the addition of water content, small nanorods were aggregated, and they had bullet-like shape with a diameter of 100 nm. When the water content increased from 12.5 to 50%, sub-micro/micrometer sized ZnO rods were obtained. Finally, when the water content was increased to 100%, several micrometers sized

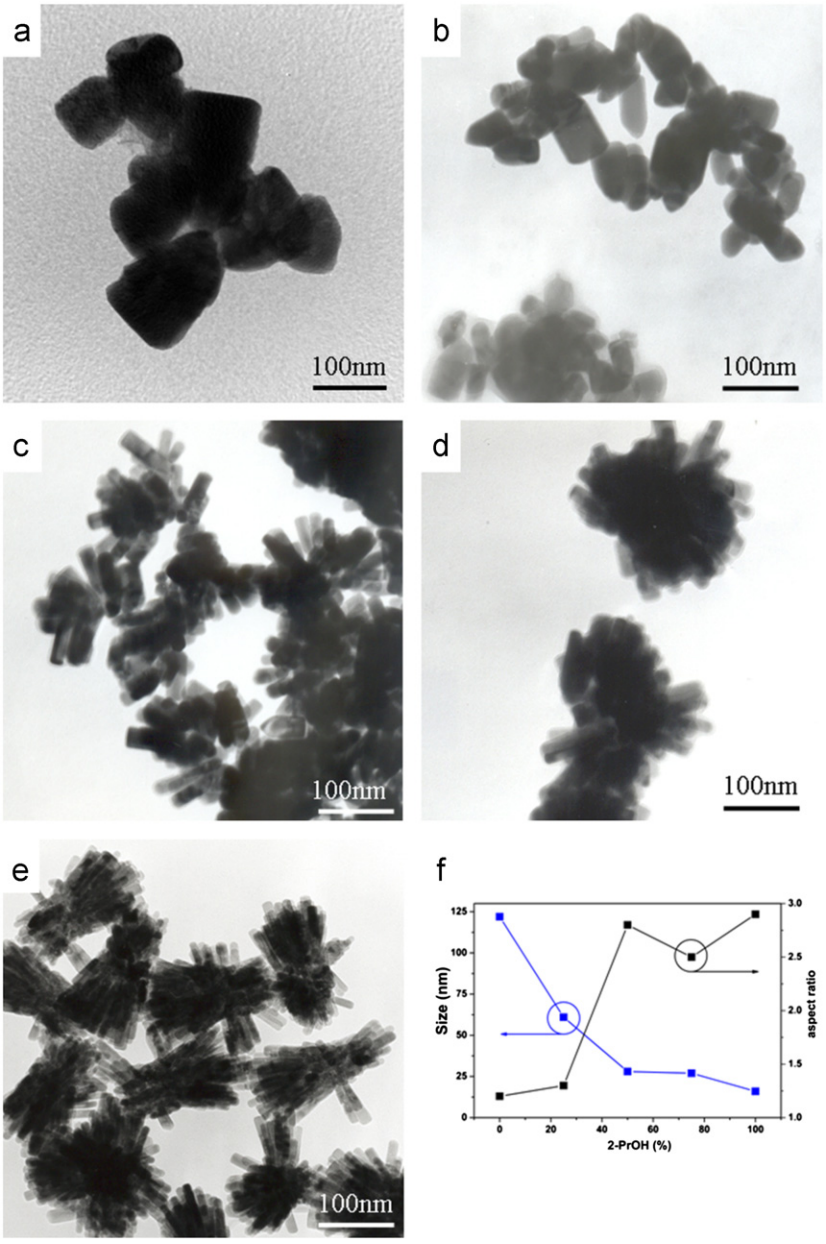

Fig. 7. TEM images of the ZnO NPs at different toluene/2-PrOH interface: (a) 100:0, (b) 75:25, (c) 50:50, (d) 25:75, (e) 0:100, and (f) (101) aspect ratio result of ZnO NPs as function of toluene/2-PrOH ratio.

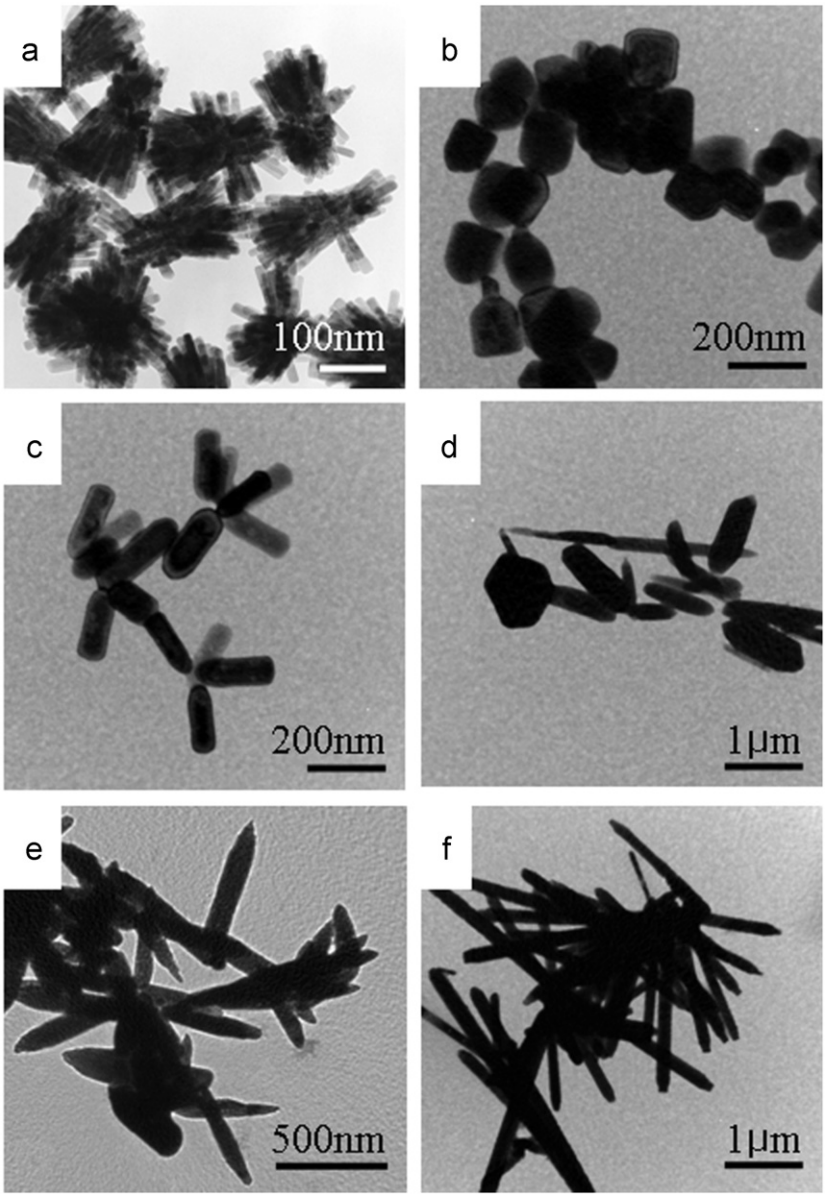

Fig. 8. TEM images of ZnO NPs at different 2-PrOH/water interface: (a) 100:0, (b) 95:5, (c) 87.5:12.5, (d) 75:25, (e) 50:50, and (f) 0:100.

ZnO rods were obtained. According to the observed results, this systematic correlation suggests that the lower polarity of solvent slow down the relative growth along the (001) direction and therefore provides a simple approach to control the aspect ratio of ZnO NPs.

4. Conclusions

Polarity of the solvents induced tunable morphologies of the ZnO NPs were successfully synthesized by a solvothermal method. The ZnO NPs have a bullet-like shape with the an aspect ratio of ≤ 2 when grown in a lower polarity solvent(< 2), and shows a nanorod shape with an aspect ratio of 2–4 when grown in the higher polarity (3–5.5) solvents. Also, the microrod shape with an aspect ratio of 10 was observed when grown in much higher polarity (water: 10.2). The morphology of ZnO NPs has been controlled easily by varying the polarity of the solvent. We believed that this is a simple approach for getting the required shape to practical application in nanodevices.

Acknowledgment

This research was supported by the Industrial Strategic Technology Development Program(Project no: 10037416) funded by the Ministry of Knowledge Economy(MKE, Republic of Korea).

References

[1] J. Tang, A.P. Alivisatos, Crystal splitting in the growth of Bi_2S_3, Nano Letters 6 (2006) 2701.

[2] Z.R. Tian, J.A. Voigt, J. Liu, B. Mckenzie, M.J. Mcdermott, M.A. Rodriguez, H. Konishi, H. Xu, Complex and oriented ZnO nanostructures, Nature Materials 2 (2003) 821.
[3] Z. Wang, X. Qian, J. Yin, Z. Zhu, Large-scale fabrication of tower-like, flower-like, and tube-like ZnO arrays by a simple chemical solution route, Langmuir 20 (2004) 3441.
[4] K. Tang, Y. Qian, J. Zeng, X. Yang, Solvothermal route to semiconductor nanowires, Advanced Materials 15 (2003) 448.
[5] W. Peng, S. Qu, G. Cong, Z. Wang, Synthesis and structures of morphology-controlled ZnO nano- and micro-crystals, Crystal Growth and Design 6 (2006) 1518.
[6] X. Han, G. Wang, L. Zhou, J.G. Hou, Crystal orientation-ordered ZnO nanorod bundles on hexagonal heads of ZnO microcones: epitaxial growth and self-attraction, Chemical Communications (2006) 212.
[7] A.K. Parchur, A.I. Prasad, A.A. Ansari, S.B. Rai, R.S. Ningthoujam, Luminescence properties of Tb^{3+}-doped $CaMoO_4$ nanoparticles: annealing effect, polar medium dispersible, polymer film and core–shell formation, Dalton Transactions 41 (2012) 11032.
[8] A.K. Parchur, A.I. Prasad, S.B. Rai, R.S. Ningthoujam, Improvement of blue, white and NIR emission in YPO_4:Dy^{3+} nanoparticles on co-doping of Li^+ ions, Dalton Transactions 41 (2012) 13810.
[9] R. Khan, A. Kaushik, P.R. Solanki, A.A. Ansari, M.K. Pandey, B.D. Malhotra, Zinc oxide nanoparticles–chitosan composite film for cholesterol biosensor, Analtica Chimica Acta 2 (2008) 207.
[10] C. Hofmann, J. Rusakova, T. Ould-Ely, D. Prieto-Centurión, K.B. Hartman, A.T. Kelly, A. Lttüge, K.H. Whitmire, Shape control of new Fe_xO–Fe_3O_4 and $Fe_{1-y}Mn_yO$–$Fe_{3-z}Mn_zO_4$ nanostructures, Advanced Functional Materials 18 (2008) 1661.
[11] J. Joo, S.G. Kown, J.H. Yu, T. Hyeon, Synthesis of ZnO nanocrystals with cone, hexagonal cone, and rod shapes via non-hydrolytic ester elimination sol–gel reaction, Advanced Materials 17 (2005) 1873.
[12] J.Y. Park, H.C. Jung, G.S. Rama Raju, B.K. Moon, J.H. Jeong, B.C. Choi, J.H. Kim, A facile synthesis of mesoporous TiO_2 spheres with hollow interiors: one-step template free synthesis via solvothermal reaction method, Journal of Electrochemical Society 159 (2012) P8.
[13] J. Ye, J. Cai, S. Chen, X. Zhao, H. Zhou, L. Qi, Nanoporous anatase TiO_2 mesocrystals: additive-free synthesis, remarkable crystalline-phase stability, and improved lithium insertion behavior, Journal of American Chemical Society 133 (2011) 933.
[14] H.J. Noh, D.S. Seo, H. Kim, J.K. Lee, Synthesis and crystallization of anisotropic shaped ZrO_2 nanocrystalline powders by hydrothermal process, Material Letters 57 (2003) 2425.
[15] A.C.C. Esteves, A.M. Barros-Timmons, J.A. Martins, W. Zhang, J. Cruz-Pinto, T. Trindade, Crystallization behaviour of new poly(tetramethyleneterephthalamide) nanocomposites containing SiO_2 fillers with distinct morphologies, Composites: Part B 36 (2005) 51.
[16] A. Umar, S.H. Kim, J.H. Kim, A. Al-Hajry, Y.B. Hahn, Temperature-dependant non-catalytic growth of ultraviolet-emitting ZnO nanostructures on silicon substrate by thermal evaporation process, Journal of Alloys and Compounds 463 (2008) 516.
[17] B. Liu, C. Zeng, Hydrothermal synthesis of ZnO nanorods in the diameter regime of 50 nm, Journal of American Chemical Society 125 (2003) 4430.
[18] L.H. Zhao, S.Q. Sun, Synthesis of water-soluble ZnO nanocrystals with strong blue emission via a polyol hydrolysis route, Crystal Engineering Communications 13 (2011) 1864.
[19] X. Zhang, X. Tao, Y. Zhao, Z. Zhang, Sonochemical method for the preparation of ZnO nanorods and trigonal-shaped ultrafine particles, Material Letters 59 (2005) 1745.
[20] M. Haase, H. Weller, A. Henglein, Photochemistry and radiation chemistry of colloldal semiconductors. 23. electron storage on ZnO particles and size quantization, Journal of Physical Chemistry 92 (1988) 482.
[21] H. Yan, J. Johnson, M. Law, R. He, K. Knutsen, J.R. McKinny, J. Pham, R. Saykally, P. Yang, ZnO Nanoribbon microcavity lasers, Advanced Materials 15 (2003) 1907.
[22] W.I. Park, Y.H. Jun, S.W. Jung, G.–C. Yi, Excitonic emissions observed in ZnO single crystal nanorods, Applied Physics Letters 82 (2003) 964.
[23] R. Guo, J. Nishimura, M. Higashihata, D. Nakamura, T. Okada, Substrate effects on ZnO nanostructure growth via nanoparticle-assisted pulsed-laser deposition, Applied Surface Science 254 (2008) 3100.
[24] S.K. Park, J.H. Park, K.Y. Ko, K.S. Chu, W. Kim, Y.R. Do, Hydrothermal-Electrochemical, Synthesis of ZnO nanorods, Crystal Growth & Design 9 (2009) 3615.
[25] X.H. Lu, D. Wang, G.R. Li, C.Y. Su, D.B. Guang, Y.X. Tong, Controllable electrochemical synthesis of hierarchical ZnO nanostructures on FTO glass, Journal of Physical Chemistry C 113 (2009) 13574.
[26] J.J. Wu, S.C. Liu, Low-temperature growth of wall-aligned ZnO nanorods by chemical vapor deposition, Advanced Materials 14 (2002) 215.
[27] W. Bai, K. Yu, Q. Zhang, F. Xu, D. Peng, Z. Zhu, Large-scale synthesis of ZnO flower-like and brush pen-like nanostructures by a hydrothermal decomposition route, Material Letters 61 (2007) 3469.
[28] S.H. Ko, D. Lee, H.W. Kang, K.H. Nam, J.Y. Yeo, S.J. Hong, C.P. Grigoropoulos, H.J. Sung, Nanoforest of hydrothermally grown hierarchical ZnO nanowires for a high efficiency dye-sensitized solar cell, Nano Letters 11 (2011) 666.
[29] M. Sathis, K. Miyazawa, Size-tunable hexagonal fullerene (C60) nanosheets at the liquid–liquid interface, Journal of American Chemical Society 129 (2007) 13816.
[30] A.K. Parchur, R.S. Ningthoujam, Preparation, microstructure and crystal structure studies of Li^+ co-doped YPO_4:Eu^{3+}, RSC Advances 2 (2012) 10854.